NUMERICAL INVESTIGATION OF SCALING EFFECTS ON THE PERFORMANCE CHARACTERISTICS OF LARGE-SCALE AXIAL FLOWS FANS

Tristan Oliver LE ROUX, Chris MEYER,
Sybrand Johannes VAN DER SPUY

Stellenbosch University, The Department of Mechanical and Mechatronic Engineering, Joubert Street, POB 7602, Stellenbosch, South Africa

SUMMARY

Large diameter Axial flow fans are predominantly used for cooling purposes, such as in air-cooled heat exchangers. Since it is difficult to experimentally test large-scale fans in the controlled environments provided by fan test facilities, smaller scaled-down versions of the fans are tested instead. Scaling laws (affinity laws) are then used to determine the performance characteristics of the large-scale fan.

The size difference between two scaled fans means that it is not possible to match their Reynolds numbers when testing with the same test fluid.

A comparison is conducted using experimental results and four numerical models for two different fans, which are scaled to different fan sizes: 0.63 m, 1.542 m, 3.6576 m and 7.3152 m, to determine the effect of the Reynolds number on the performance characteristics of an axial flow fan. The numerical geometries are based on the M- and B2a-fan, and are tested in the A-type experimental setup fan test facility at Stellenbosch University, which is used to obtain the experimental results.

It was found that as the fan size increases, and thus the Reynolds number increases, the performance characteristics improve and tend toward their performance limits, which correlates with the Reynolds number effect on the lift and drag properties of aerofoils.

INTRODUCTION

Axial flow fans are predominantly used for cooling purposes. One such application is within air-cooled heat exchangers. Since wet-cooled alternatives require a considerable amount of water to operate, air-cooled systems reduce the water consumption while still providing a cost-effective substitute [1]. Thus, in regions with dry climates where water is scarce, air-cooled heat exchangers are a preferable alternative to wet-cooled systems. Air-cooled heat exchangers are therefore very convenient for use in concentrated solar power (CSP) plants, as these are typically located within deserts or arid regions with high solar potential but limited water resources [2].

Air-cooled heat exchangers operate by using an array of axial flow fans, which move large amounts of air through heat exchanger bundles. This allows for the rejection of energy to the environment in the form of heat using convection. Since it is difficult to experimentally test large-scale fans in the controlled environments provided by fan test facilities, smaller scaled-down versions of the fans are tested instead. Scaling laws (affinity laws) are then used to determine the performance characteristics of the large-scale fan. The size difference between two scaled fans means that it is not possible to match their Reynolds numbers when testing with the same test fluid. Since the Reynolds number describes the relationship between inertial and viscous forces, a difference in Reynolds number between two fans of different sizes leads to non-identical behaviour of the boundary layers on the fan blades, which produce different performance characteristics. It is therefore important to determine and quantify the effect that the Reynolds number has on the accuracy of predicting the performance characteristics of scaled-down axial flow fans.

Pelz et al. [3] conducted research on a new scaling method aimed at omitting empirical functions in scaling to develop a universal, physically-based scaling method. The scaling method is a modification of the scaling formulation derived by Pelz and Hess [4], based on the assumption that inertia losses in the model consist of two parts: scaling the efficiency and subsequently the flow coefficient. However, a shortcoming of Pelz et al.'s [3] work is that it does not extend to the large diameters of fans typically considered for cooling applications.

FAN SPECIFICATIONS

The axial flow fan used in this paper is the M-fan designed by Wilkinson [5] and B2a-fan by Bruneau [6]. Four different diameter versions of the each fan are used, namely 7.3152 m, 3.6576 m, 1.542 m, and 0.63 m. Therefore, it is important to scale down the operating conditions from the 7.315 m diameter fan to match those of the 3.6576 m, 1.542 m, and 0.63 m version. It was decided to scale the fans down using the shroud diameter instead of the rotor diameter; however, the tip gap was kept constant at 0.259% of the shroud diameter. The following table details the operating specifications of the M- and B2a-fan at a diameter of 1.542 m.

Table 1: Fan Operating Specifications

	Units	M-Fan	B2a-Fan
Number of Blades	–	8	8
Hub-to-Tip Ratio	–	0.289	0.4
Casing Diameter	m	1.542	1.542
Volume Flow rate	m^3/s	14.797	16
Fan Static Pressure Rise	Pa	116.7	210
Blade Tip Speed	m/s	58	60.55
Rotational Speed	rpm	718.36	750
Shaft Power	W	2812	6000
Fan Static Efficiency	%	61.4	56
Density	kg/m^3	1.209	1.209

EXPERIMENTAL TESTING

The performance of the M-fan and B2a-fan were evaluated by experimentally measuring the pressure rise, efficiency, and power consumption characteristics as a function of the volumetric flow rate. This experimental analysis is required to validate the analytical and numerical models. The experimental testing is conducted within a type A (free inlet and outlet) 1.542 m diameter wind tunnel at the Mechanical and Mechatronic Engineering Department at Stellenbosch University. The procedure is performed according to the ISO 5801 standards [7], which deals with performance testing of fans using standardized airways.

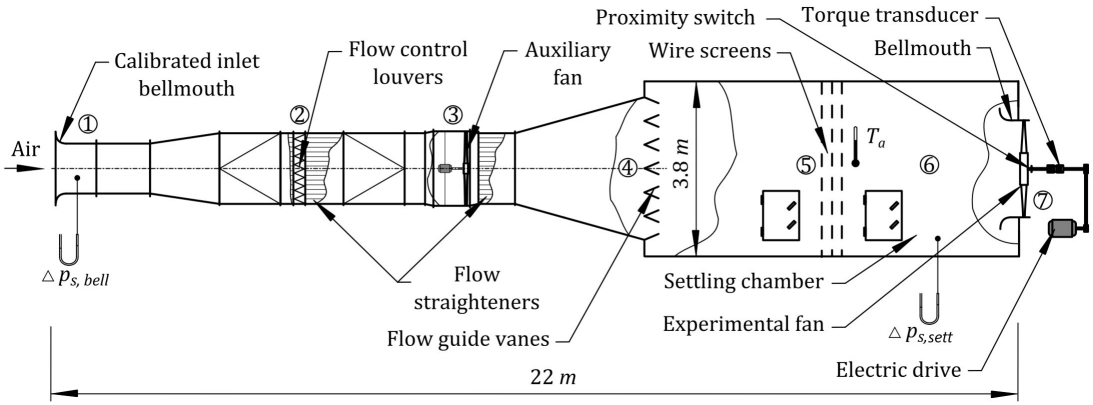

Figure 1: Stellenbosch University BS 848, Type A Fan Test Facility ([8])

NUMERICAL MODEL

The performance characteristics of the M-fan and B2a-fan is modeled at a range of flow rates and blade setting angles to verify and quantify the performance characteristics of the M-fan.

Computational Domain

The P3DM computational domain consists of three sub-domains, the inlet, outlet, and rotor sub-domain, with two sets of non-conformal periodic interfaces coupling the inlet and outlet meshes to

the rotor mesh. Having three individual subdomains allows for flexible grid resolution based on localized pressure gradients while also saving on computational processing where necessary [9]. All three meshes are constructed using poly-hexcore cells, which combine octree hexahedrons (for bulk regions), poly-prisms (for boundary layers), and polyhedra (for interfaces between octree hexahedrons and poly-prism cells) to create a mesh within Ansys Fluent Mesher. Each subdomain contains a periodic pair and is configured with a rotational matching periodic boundary condition at an angle of 45°.

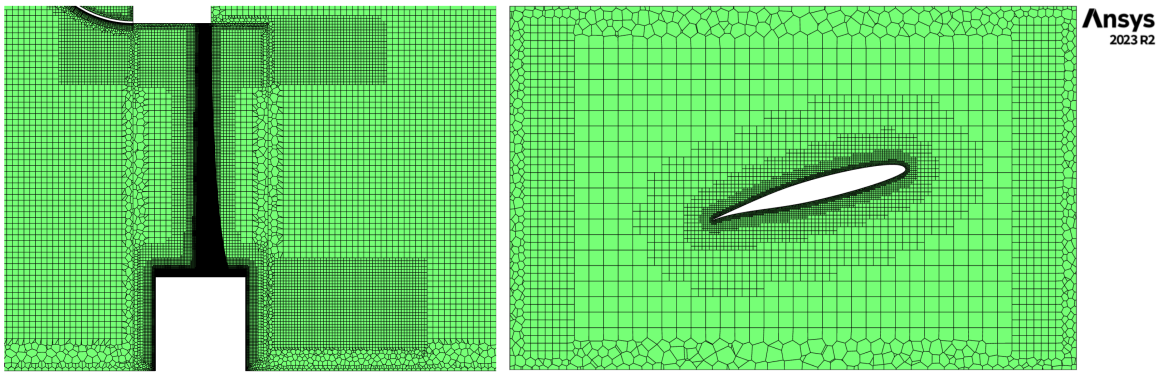

Figure 2: P3DM Rotor Mesh

The method used to model the flow through the three subdomains is the Multiple Reference Frame Model (MRF) model. The MRF model is a steady-state approximation in which individual domains rotate around different axes and/or rotational speeds. Each sub-domain is solved by calculating the relative flow in its chosen reference frame. Special treatment of the interfaces between the different sub-domains is required to allow for the boundary conditions to have the correct reference frame.

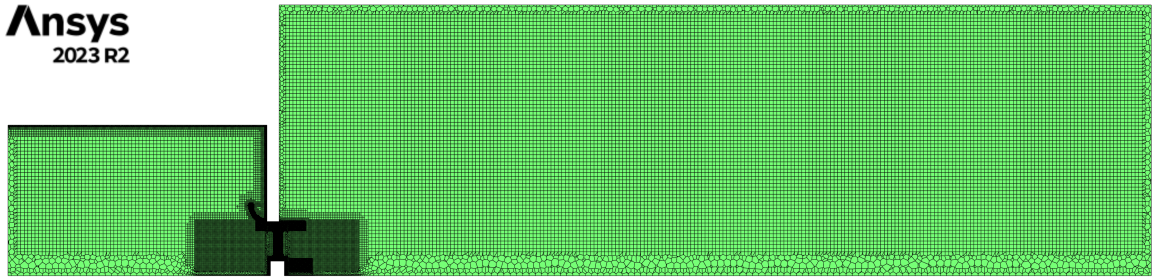

Figure 3: P3DM Computational Domain

The rotor sub-domain is composed of an angular segment that encloses the blade profile and hub and is situated between the inlet and outlet sub-domain. An inflation layer is applied to the blade, shroud, hub, and bellmouth to constrain the y^+ values along the blade length to accommodate the different turbulent models y^+ requirement. A grid independence study was conducted, and it was determined that a cell count of approximately 8.8×10^6 was sufficient for convergence for all four fan diameters. The inlet and outlet sub-domain boundary lengths are determined through a sensitivity analysis. To achieve sufficient convergence, the lengths are set to $z_i = 2.406d_c$ and $z_o = 8d_c$, respectively.

Boundary Conditions

Since the P3DM consists of a one-eighth segment of the M-fan and B2a-fan, each sub-domain contains a periodic pair and is configured with a rotational matching periodic boundary condition at an angle of 45°. When combining the three sub-domains into one computational domain, two non-conformal periodic repeats mesh interfaces are created to join the rotor sub-domain to the inlet and

outlet sub-domains. A non-conformal interface applies an interpolation scheme between the two surfaces, allowing all relevant properties to transfer from one sub-domain to the other.

The inlet is defined as a velocity inlet, with flow entering the domain normal to the boundary in the negative z-direction. This allows for a constant flow distribution at the inlet of the domain. The outlet is defined as a zero gauge static pressure outlet, while the backflow is set normal to the boundary with a static pressure specification. The flow turbulence is specified to enter the inlet and leave the outlet with an intensity of 3%, while the length scale is shown in Table 2:

Table 2: M-Fan Turbulence Length Scale

Casing Diameter	7.315 m	3.657 m	1.542 m	0.63 m
Length Scale	0.047 m	0.024 m	0.01 m	0.004 m

The inlet and outlet sub-domains are specified as having a stationary reference frame, while the rotor sub-domain is specified as having a rotational reference frame with a rotational speed about the negative z-axis in the absolute coordinate scheme.

All surfaces in the three sub-domains are specified to have a no-slip wall boundary condition. The shroud in the rotor sub-domain functions as a moving wall, with zero rotational speed in the absolute reference frame. The two blades, three hubs, and two shroud surfaces in the inlet and outlet sub-domains are designated as stationary walls, as they remain stationary relative to the flow's rotation.

Turbulence Modelling

Several turbulence models were compared using the base M-fan, and it was found that the $k-\omega$ SST model provided the most accurate results across the following y^+ ranges on the rotor for the four fan diameters:

Table 3: M- and B2a-Fan Y^+ *Ranges*

Casing Diameter	7.315 m	3.657 m	1.542 m	0.63 m
Minimum y^+	1.821	1.157	0.707	0.523
Maximum y^+	109.1	53.05	53.12	40.6
Initial Layer Height	0.95 mm	0.4 mm	0.4 mm	0.2942 mm
Cell Count	$8.76x10^6$	$8.85x10^6$	$8.17x10^6$	$8.32x10^6$

Solver Settings

The discretization schemes and solver settings are shown in Table 4 and are selected based on work done by Wilkinson [5] and Louw [8]. Table 4 represents the solver settings for the k-ω SST model.

Table 4: P3DM Solver Settings

Pressure-Velocity Coupling	SIMPLE
Flux Type	Rhie-Chow: Momentum Based
Discretization Scheme (Gradient)	Least Squares Cell Based
Discretization Scheme (Pressure)	PRESTO!
Discretization Scheme (Momentum)	QUICK
Turbulent Kinetic Energy	QUICK
Specific Dissipation Rate	QUICK
Pseudo Time Method	Off
Warped-Face Gradient Correction	On

Warped-face gradient correction was enabled, which improves gradient accuracy by addressing high aspect ratios, non-flat-faced cells in boundary layers, and highly deformed cells. However, it was found to have no effect on the simulation results, although it increased the rate of convergence. All under-relaxation factors were kept to their default values proposed by Ansys [10], while all residual convergence limits are set to 1e-5.

RESULTANT EFFECTS ON FAN SCALING

From the numerical results, the influence of the fan diameter on fan behavior is investigated for a range of volume flow rates ($12-19 m^3/s$). These effects are compared using the total-to-static pressure rise, shaft power, and total-to-static efficiency. The experimental results are displayed both as raw data and poly-fitted curves from several sets of experimental data for the fan's pressure, power, and efficiency curves. The performance characteristics of the M-Fan and B2a-Fan with a 0.259% (4 mm for the 1.542 m fan) tip gap at their design hub angles are discussed to determine the accuracy of the P3DM.

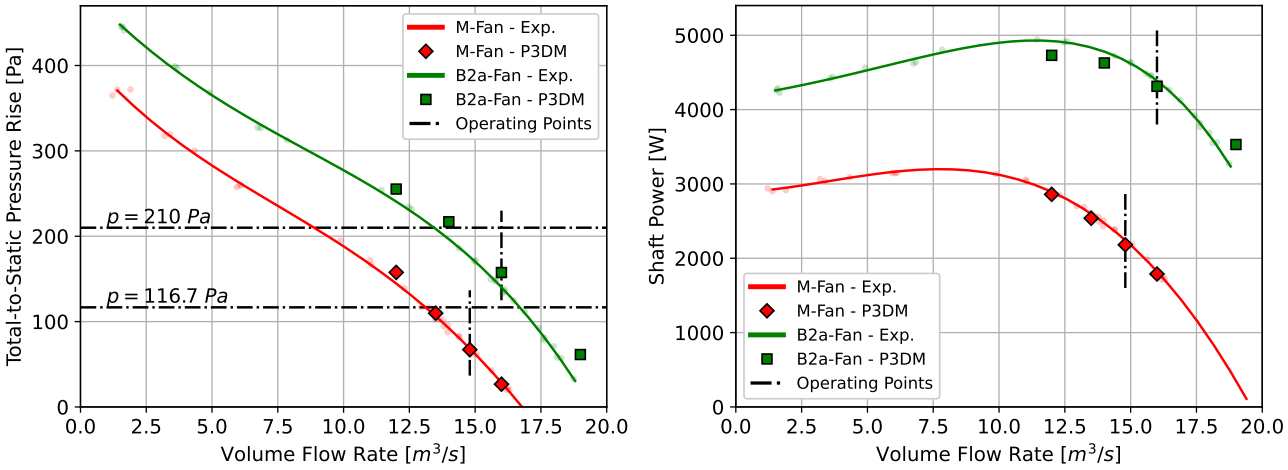

Figure 4: M-Fan and B2a-Fan Performance Characteristics

Comparing the experimental pressure rise of the M-Fan to the P3DM for the 1.542 m fan shows a strong correlation across the full range of simulated volume flow rates, while the numerical results of the B2a-Fan overpredict the pressure rise by an average of 8.66%. The comparison between the experimental and numerical shaft power for the M-Fan shows a strong correlation, while the B2a-Fan

underpredicts power at flow rates lower than the design and overpredicts it at higher flow rates.

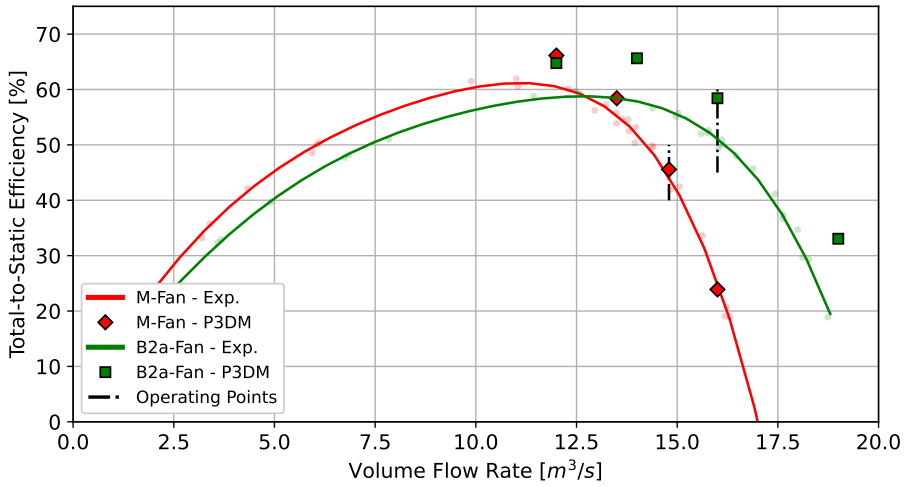

Figure 5: Total-to-Static Efficiency

The total-to-static efficiency depends on the pressure and power characteristics of the fan. As such, the trends and errors seen in Figure 4 are carried over to the efficiency and are visible in Figure 5. As seen in Figure 5, due to the underprediction of shaft power and the overprediction of the pressure rise, the P3DM overpredicts the efficiency of the B2a-Fan. Meanwhile, the P3DM accurately predicts the total-to-static efficiency of the M-Fan across the full range of flow rates.

The performance characteristics at the design flow rate versus Reynolds number at the blade tip for the M- and B2a-fan are shown in Figure 6 and Figure 7. The pressure rise for all four fan diameters were scaled to 1.542 m and then normalized by the pressure rise of the 1.542 m fan. The same method was applied to the shaft power and efficiency. This was done to compare the change in pressure rise, power, and efficiency relative to each other, since the M-fan and B2a-fan have vastly different pressure rise and power consumption values.

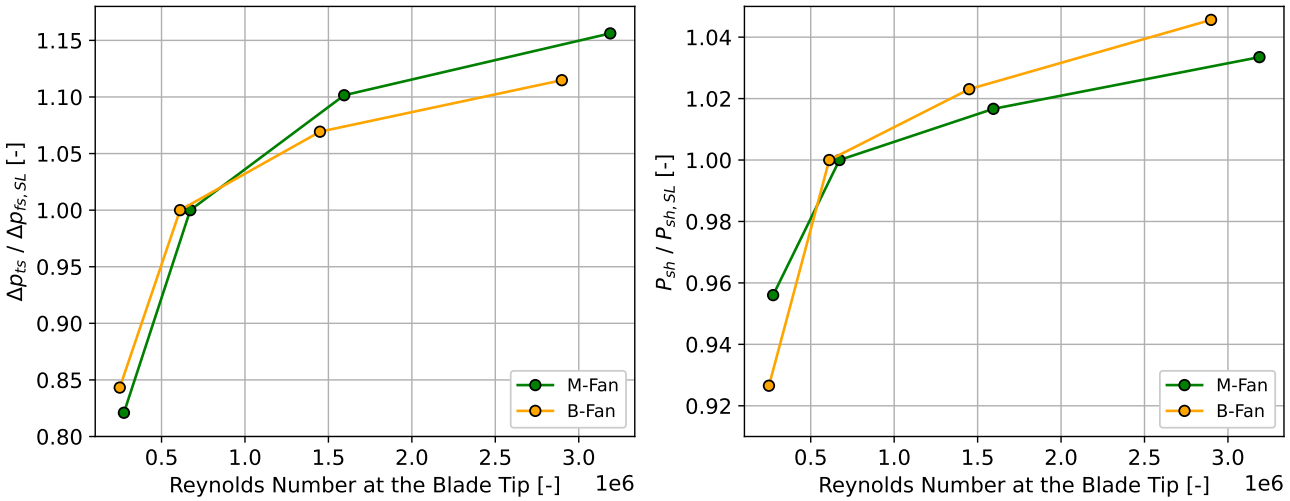

Figure 6: Effect of Reynolds Number on the Performance Characteristics

It was found that when scaling larger axial flow fans, with only a small increase in Reynolds numbers, the method proposed by Pelz et al. [3] becomes inaccurate. The method still held true when scaling up from 0.63 m to 1.542 m, with only a 1.75% difference in efficiency and a 1.5 Pa difference in pressure rise when comparing the scaled-up P3DM results for 0.63 m to the 1.542 m P3DM results.

However, when scaling up from 1.542 m and 3.6576 m to 7.3152 m, a difference of 10 to 14 Pa in pressure rise and 7 to 11% in efficiency was observed.

For both fans, there is a general increase in fan static pressure, power, and efficiency with an increase in fan size and thus Reynolds number, at constant flow rates. However, as fan size and Reynolds number increase, the improvement in fan performance characteristics diminishes. The performance characteristics are then said to be independent of the Reynolds number.

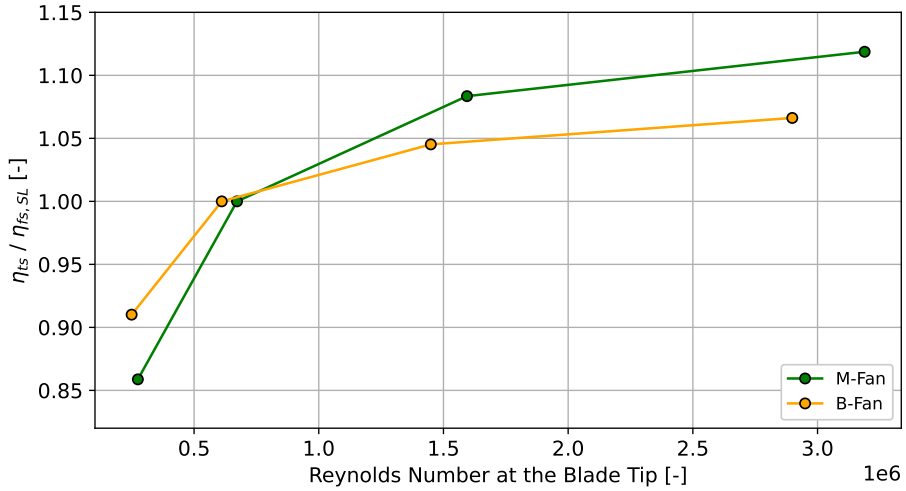

Figure 7: Effect of Reynolds Number on the Fan Efficiency

According to the affinity laws, the efficiency of the different-sized fans should be equal. In reality, this is not the case, since the affinity laws neglect viscous effects and changes in Reynolds number. As the Reynolds number increases, the effect of viscous losses, such as surface friction, decreases. In turn, inertia losses, such as tip clearance losses, dominate. This results in the logarithmic trend of Reynolds number on fan performance characteristics, as seen in the figures above.

The following aerofoil properties for the NASA 0413 were obtained from XFoil by Drela and Youngren [11] with an N_{crit} value of 0.1, as it has been proven to give improved results for low angles of attack below the stall point [5]. The following figures show the effect that the Reynolds number has on the lift at the hub of the M-Fan, which has an angle of attack of 2.85°, for the 7.315 m ($Re_{hub} = 9.5 \times 10^5$) and 0.63 m ($Re_{hub} = 8.14 \times 10^4$) diameter fans. There is a 15.16% drop in lift and an 84.62% increase in drag at the hub of the fan when reducing the fan diameter from 7.3152 m to 0.63 m. For the tip, which has a Reynolds number of 3.19×10^6 for 7.3152 m fan and 2.75×10^5 for 0.63 m fan, there is a 2.78% drop in lift and a 61.08% increase in drag at an angle of attack of 0.67°.

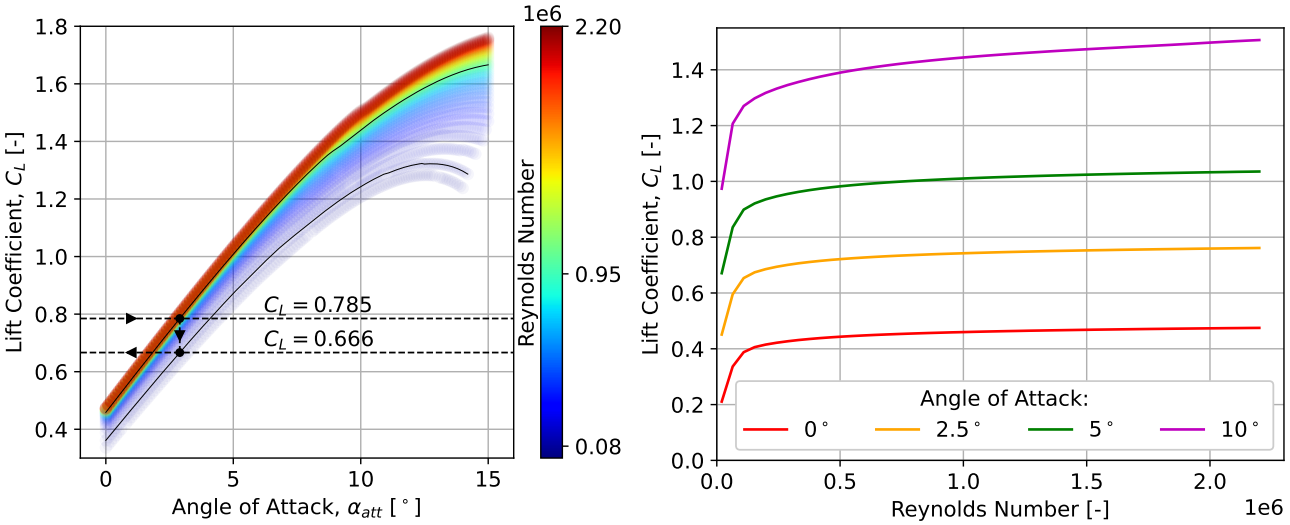

Figure 8: Reynolds Number Effects on the Lift Coefficient

As the Reynolds number increases, the lift tends to follow the same characteristic curve, as seen in Figure 8. Lift, not drag, is the primary contributor to both pressure rise and power, and, in conjunction, they define efficiency. This shows that, as the fan diameter increases, the effect of an increase in Reynolds number on the fan decreases, which was observed with the performance characteristics of the M-Fan and B2a-Fan at different fan diameters.

CONCLUSION

Fan performance over a range of flow rates for 0.63 m, 1.542 m, 3.6576 m and 7.3152 m diameter M- and B2a-fans was assessed to determine the effect that fan size and Reynolds number have on an axial flow fan. It was found that the trends observed between the two different types of fans are consistent and show that an increase in pressure rise, power consumption, and total-to-static efficiency occurs with an increase in fan size and subsequently Reynolds number. As the diameter increases, and thus Reynolds number increases, the performance characteristics tend to approach their performance limits. Similar trends are observed in the effect that Reynolds number has on the lift and drag characteristics of aerofoil profiles.

REFERENCES

[1] D. G. Kröger, *Air-cooled Heat Exchangers and Cooling Towers*. Department of Mechanical Engineering, Stellenbosch University: Self Published, **2004**.

[2] T. O. Meyer, "Design of a tip appendage for the control of tip leakage vortices in axial flow fans," Ph.D. dissertation, Mechanical Engineering, Stellenbosch University, South Africa, **2021**.

[3] P. F. Pelz, S. Stonjek, and B. Matyschok, *The influence of reynolds number and roughness on the efficiency of axial and centrifugal fans.* Journal of Engineering for Gas Turbines and Power vol. 135, **2012**.

[4] P. F. Pelz and M. Hess, *Scaling friction and inertia losses for the performance prediction of turbomachines.* 13th International Symposium on Transport Phenomena and Dynamics of Rotating Machinery (ISROMAC-13) vol. 122, **2010**.

[5] M. B. Wilkinson, "The design of an axial flow fan for air-cooled heat exchanger applications," M.S. thesis, Mechanical Engineering, Stellenbosch University, South Africa, **2017**.

[6] P. R. P. Bruneau, "The design of a single rotor axial flow fan for a cooling tower application," M.S. thesis, Mechanical Engineering, Stellenbosch University, South Africa, **1994**.

[7] *Industrial fans - performance testing using standardized airways*, 2nd ed., International Standard, **2007**.

[8] F. G. Louw, "Investigation of the flow field in the vicinity of an axial flow fan during low flow rates," Ph.D. dissertation, Mechanical Engineering, Stellenbosch University, South Africa, **2015**.

[9] J. N. Rohwer, "Blade surface pressure measurements of an axial flow fan," M.S. thesis, Mechanical Engineering, Stellenbosch University, South Africa, **2019**.

[10] *Ansys fluent user's guide*, Release 18.1, **2017**.

[11] M. Drela and H. Youngren, *Xfoil 6.94 user guide*, **2001**.